This document is downloaded from DR-NTU, Nanyang Technological University Library, Singapore.

Title	Observation of clusters in Re60Fe30Al10 alloys and the associated magnetic properties
Author(s)	Kong, H. Z.; Ding, Jun; Dong, Zhili; Wang, L.; White, Timothy John; Li, Y.
Citation	Kong, H. Z., Ding, J., Dong, Z. L., Wang, L., White, T., & Li, Y. (2002). Observation of clusters in Re60Fe30Al10 alloys and the associated magnetic properties. Journal of Physics D: Applied Physics, 35(5), 423-429.
Date	2002
URL	http://hdl.handle.net/10220/8296
Rights	© 2002 Institute of Physics Publishing. This is the author created version of a work that has been peer reviewed and accepted for publication by Journal of Physics D: Applied Physics, Institute of Physics Publishing. It incorporates referee's comments but changes resulting from the publishing process, such as copyediting, structural formatting, may not be reflected in this document. The published version is available at: [DOI: http://dx.doi.org/10.1088/0022-3727/35/5/302]

Observation of clusters in $Re_{60}Fe_{30}Al_{10}$ alloys and the associated magnetic properties

Kong H Z[1], Ding J[1,4], Dong Z L[2], Wang L[3], White T[2] and Li Y[1]

[1] Materials Science Department, National University of Singapore, Singapore 119260
[2] Environmental Technology Institute, Innovation Center, Nanyang Technology University, Singapore 637723
[3] Physics Department, National University of Singapore, Singapore 119260
[4] Author to whom correspondence should be addressed. E-mail: masdingj@nus.edu.sg

ABSTRACT

Magnetic properties and microstructure of melt-spun ribbons of $RE_{60}Fe_{30}Al_{10}$ alloys with RE = Nd, Sm, Dy, Gd and Y were studied in detail. High coercivity values in the range of MA m^{-1} were observed at low temperatures for amorphous ribbons. Presence of Fe-rich clusters and nanoscale rare-earth crystallites in the amorphous matrix in the ribbons were revealed by high-resolution transmission electron microscopy studies. The magnetic transition temperatures were estimated experimentally and compared with fitting results based on the cluster ferromagnetism model (Wang L et al 2001 Phys. Rev. B **64** 214410). Possible mechanisms for the magnetic behaviour observed due to the presence of Fe-rich magnetic clusters are discussed.

1. INTRODUCTION

The structural disorder in amorphous magnetic materials has generated a number of interesting magnetic properties such as high Curie temperature, magnetostriction and induced anisotropy, which can be tailored for different applications [2]. The amorphous rare-earth–transition-metal films deposited by magnetron sputtering, e.g. GdTb–Fe, Tb–FeCo and Dy–FeCo, are promising candidates for magneto-optical information storage due to their large perpendicular anisotropy and high Curie temperature [2]. Different origins were proposed to account for the observed anisotropy, e.g. structural inhomogeneities [3], stress-induced anisotropy [4], dipolar interactions [5] and exchange anisotropy [6].

More recently, high coercivity combined with outstanding glass forming ability was observed for (Nd, Pr)–Fe–Al alloys [7]. The hard magnetic properties were suggested to be due to magnetic exchange coupling interaction among the Fe-rich clusters with large random magnetic anisotropy in the relaxed amorphous samples [7]. Fine dark and bright patches of 1–2 nm in diameter spread uniformly in the amorphous $Pr_{90}Fe_{10}$ alloy were observed under high-resolution transmission electron microscope (HRTEM) [8]. The fine patches were correlated to ferromagnetic clusters [8]. Results from our previous studies on magnetic behaviour of the amorphous ribbons of rare-earth–iron (RE–Fe)-based alloys [9–12] also suggested presence of Fe-rich magnetic clusters in these ribbons.

The complex magnetic behaviour observed by Ortega-Hertogs *et al* [13] for bulk glassy rods (2.7mm in diameter) of $Nd_{60}Fe_{30}Al_{10}$ alloy shows that in a temperature region where the ribbon is paramagnetic, the hysteresis loop is well simulated by a Stoner–Wohlfarth type of loop, supporting the existence of an ensemble of ferromagnetic entities with uniaxial anisotropy, whose easy axes are oriented at random, and remain magnetically isolated by a paramagnetic matrix, the Nd-rich phases [13]. At 2.6 K, the Nd-rich matrix into which the Fe-rich Fe-Nd entities are embedded is antiferromagnetic. The Fe-Nd entities become magnetically coupled to the surrounding Nd-rich matrix via Fe-Nd and Nd–Nd exchange interaction, and the Nd-rich matrix is expected to develop a large crystal field anisotropy [13]. A magnet that is structurally glassy but magnetically granular at the nanoscale and exhibits good isotropic hard magnetic properties is suggested [13].

Recently, we proposed a model (named the cluster ferromagnetism model) to account for the unique magnetic behaviour of these inhomogeneous amorphous RE–Fe-based ribbons [14]. The magnetic units in this model are magnetic clusters with random distribution of magnetic easy directions, and with strong interaction between the clusters. The model can be expressed in the Hamiltonian here:

$$E = -D\sum_i [\vec{n}_i \cdot \vec{m}_i(T)]^2 - \frac{1}{2}\sum_{i \neq j} J_{ij}[\vec{m}_i(T) \cdot \vec{m}_j(T)] - H\sum_i \vec{m}_i(T) \quad (1)$$

where $m(T)$ is the magnetic moment of the cluster at temperature T, D is the magnetic anisotropy of a cluster, J_{ij} is the exchange interaction coefficient between the ith cluster and jth cluster, n_i is a random unit vector representing the local axis of easy magnetization direction. H is the applied magnetic field. $m(T)$ can be expressed as $m_s f(T/T_c^{\text{cluster}})$, where m_s is the saturation magnetization of the cluster phase at zero temperature or total magnetic moment of a cluster, and T_c^{cluster} is the Curie temperature of the magnetic clusters. The sample is paramagnetic at temperatures above T_c^{cluster} [14]. The Monte Carlo method has been used to simulate magnetization curves after zero-field cooling and magnetic hysteresis loops at different temperatures [1]. The simulation results showed the presence of another two critical temperatures, T_{block} and T_c^{system}. T_{block} is the blocking temperature due to anisotropy energy, while T_c^{system} is the freezing temperature due to interaction between the clusters [1]. At temperatures below T_c^{system}, remanence increases significantly due to cluster interactions that lead to ferromagnetic coupling between clusters. However, the coercivity remains low due to relatively high thermal energy in comparison to magnetic anisotropy energy, which results in easy flip of magnetization vectors. High coercivity requires the freezing of the ferromagnetic state at temperatures below T_{block} [1]. The Monte Carlo simulation work suggested that if T_c^{system} is higher than T_{block}, valid for most amorphous RE and transition metal alloys, the magnetic behaviour as a function of temperature could be divided into four periods [1]:

(a) $T_c^{cluster} < T$: paramagnetic
(b) $T_c^{system} < T < T_c^{cluster}$: superparamagnetic
(c) $T_{block} < T < T_c^{system}$: ferromagnetic with low coercivity
(d) $T < T_{block}$: ferromagnetic with high coercivity

In this paper, we have performed systematic structural and magnetic studies on amorphous ribbons of $RE_{60}Fe_{30}Al_{10}$ alloys with RE = Y, Nd, Sm, Gd and Dy. The unique magnetic behaviour and results of microstructure studies that lead to observation of clusters in these ribbons are summarized.

2. EXPERIMENTAL PROCEDURES

Ingots of nominal compositions $RE_{60}Fe_{30}Al_{10}$ with RE = Nd, Y, Sm, Gd and Dy were prepared by arc-melting the pure constituents (purity 99.5%) under argon atmosphere. Small pieces of the ingots were then re-melted and melt-spun into ribbons using single roller (copper) chill block melt-spinner at wheel surface speeds of 5 and 30 m s^{-1}. Part of the ingots was also used for casting into cylinders of diameter 1 mm and length 30 mm by low-pressure copper mould chill casting. The phases present in the samples were determined by x-ray diffraction (XRD) technique with Cu K_α radiation. Magnetic measurements were carried out by vibrating sample magnetometer (VSM) at different temperatures from 5 to 700 K. Microstructure studies were carried out using TEMs operating at 100 and 300 keV.

3. RESULTS

3.1. Structural studies

XRD patterns of ribbon melt-spun at 30 m s^{-1} (figure 1) of $Nd_{60}Fe_{30}Al_{10}$ alloy and $Sm_{60}Fe_{30}Al_{10}$ alloy show only large amorphous hump, while those of $Dy_{60}Fe_{30}Al_{10}$ alloy and $Gd_{60}Fe_{30}Al_{10}$ alloy show a small diffraction peak corresponding to their respective RE phase. Decreasing the melt-spinning speed to 5 m s^{-1} resulted in the formation of respective RE phase with preferred orientation along the (002) and small amount of RE-Al phases, e.g. Al_2Gd and $AlNd_3$ phase.

Microstructure of the ribbon of $Dy_{60}Fe_{30}Al_{10}$ alloy melt-spun at 30 m s^{-1} was studied by TEM operating at 100 keV. TEM bright field images of the ribbon melt-spun at 30 m s^{-1} (figure 2(a)) shows a generally featureless contrast typical of amorphous phase. Glassy nature of the ribbon was also confirmed by the observation of halo ring in the diffraction pattern (figure 2(b)). Upon careful studies, the micrograph revealed the presence of pastel grey shades, indicating inhomogeneity of the amorphous phase and the possible existence of clusters in the ribbon. TEM micrographs of the ribbon melt-spun at 5 m s^{-1} show the presence of large crystallites (about 100 nm) corresponding to the RE phase (in this case, Dy phase) existing in the amorphous matrix.

Ribbon of $Dy_{60}Fe_{30}Al_{10}$ alloy melt-spun at 5 ms^{-1} was further studied by HRTEM operating at 300keV. HRTEM image (figure 3) of the region classified as amorphous

under conventional TEM shows the presence of small patches of fringes around 3.4 nm in diameter scattered in the amorphous matrix. The spacing of the fringes was around 3.2 Å, which is very close to the *d*-spacing of the (100) plane of the Dy phase (3.11 Å). The precipitation of Dy phase in the amorphous matrix is highly probable since Dy make up a large proportion (more than half) of the alloy. The presence of Dy phase in the ribbon was also supported by the XRD results. The presence of circular white patches around 2.5 nm in diameter were also noticed. There are two possibilities. The first possibility is that these may be due to thickness variation inherent from the melt-spinning process or the ion-milling process during the TEM sample preparation. The size of these patches seemed too small to be caused by un-precision fabrication technique. Difference in atomic weight of the constituting atoms of a feature is another very likely source of contrast in an HRTEM image. The second possibility is hence a variation in the ratio of atoms with high atomic weight (Dy) and atoms with low atomic weight (Fe). These patches were whitish, an indication of possible higher content of the atoms with lower atomic weight such as Fe, as compared to the general amorphous matrix which consists of a large amount of heavy Dy. X-ray energy dispersive spectroscopy (EDX) analysis indicated that the whitish region in the ribbon was Fe-rich. Careful studies of the circular white patches show that they were agglomerates of atoms without any ordered arrangement, i.e. amorphous clusters. Presence of Fe-rich amorphous clusters in the ribbons is concluded.

3.2. Magnetic studies

Hysteresis loops at different temperatures for the ribbons of $Dy_{60}Fe_{30}Al_{10}$ alloy melt-spun at 30 m s^{-1} are shown in figure 4. At room temperature (290 K), the magnetization curve of the ribbon was a straight line, typical for paramagnetic material. As the temperature decreased to 170 K, the ribbon became superparamagnetic. Observation of superparamagnetism suggested the presence of clusters in the amorphous ribbon. When the temperature decreased to below 140 K, the ribbon exhibited ferromagnetism with low coercivity (H_c) (38.84 kA m^{-1} at 80K). Coercivity of the ribbon increased rapidly as temperature decreased further, reaching a high coercivity of 1992.4 kA m^{-1} at 4.2K. The amorphous ribbons of $RE_{60}Fe_{30}Al_{10}$ alloys with RE as Nd and Sm also exhibit similar series of magnetic behaviour transitions as temperature decreases, i.e. (a) above its Curie temperature, the ribbon is paramagnetic; (b) below this Curie temperature, the ribbon is superparamagnetic; (c) at still lower temperatures, the ribbon becomes ferromagnetic; (d) as temperature further decreases, the ribbon transforms from soft magnetic to hard magnetic. This phenomenon agrees well with the expectation of the cluster ferromagnetism model characterized by three critical transition temperatures, T_{block}, T_c^{system} and T_c^{cluster} (as elaborated in section 1).

Temperature dependence of inverse susceptibility ($1/\chi$) of the ribbon of $Dy_{60}Fe_{30}Al_{10}$ alloy melt-spun at 30 ms^{-1} is shown in figure 5(a). It is noticed that instead of a sharp kink signifying the transition from ferromagnetic to paramagnetic state, the inverse susceptibility traced out a gradual bowed curve, extended for about 100 K, a unique characteristic of superparamagnetic state due to the presence of clusters. T_c^{system} being the temperature at which the sample transforms from ferromagnetic to superparamagnetic

state is characterized by the temperature at which inverse susceptibility deviates from zero (as shown in figure 5(a)). T_c^{cluster} being the transition temperature from superparamagnetic state is, on the other hand, the lowest temperature at which the inverse susceptibility value follows the linearity defined by the Curie–Weiss law.

According to the results of our Monte Carlo simulation in [1], T_c^{system} can also be characterized by the temperature at which the remanence increases, as illustrated in figure 5(*b*) for the ribbon of $Dy_{60}Fe_{30}Al_{10}$ alloy melt-spun at 30 ms^{-1}. T_{block}, on the other hand, is defined experimentally by the peak of typical cusp in the ZFC curves near the temperature at which the bifurcation of the ZFC and FC curves occurs, as shown in figure 5(*d*). According to the results of our Monte Carlo simulation, T_{block} can also be characterized by the temperature at which the coercivity value starts to increase rapidly (figure 5(c)). The increase of coercivity at temperatures below T_{block} is also expected according to the equation below for spherical single-domain particles [15]:

$$H_c = \left(\frac{2K}{M_s}\right)\left[1 - \left(\frac{T}{T_{\text{block}}}\right)^{1/2}\right] \qquad (2)$$

The values of T_{block}, T_c^{system} and T_c^{cluster} as estimated for the ribbon of $Dy_{60}Fe_{30}Al_{10}$ alloy and ribbons of other $RE_{60}Fe_{30}Al_{10}$ alloys are tabulated in table 1 and plotted for different RE elements in figure 6. T_c^{system} and T_c^{cluster} of the ribbons melt-spun at 5m s^{-1} were always higher than those of the ribbons of the same alloy melt-spun at 30 ms^{-1}. Ribbon of $Nd_{60}Fe_{30}Al_{10}$ alloy gave the highest T_{block}, T_c^{system} and T_c^{cluster} among all the ribbons melt-spun at 30 m s^{-1}. T_c^{system} of $Y_{60}Fe_{30}Al_{10}$ ribbons were always the lowest. T_c^{cluster} of ribbon melt-spun at 5ms^{-1} of $Gd_{60}Fe_{30}Al_{10}$ alloy was the highest among all the ribbons melt-spun at the same speed.

Similar sequence of magnetic transition were also observed as temperature decreases when Al in $Nd_{60}Fe_{30}Al_{10}$ alloy is replaced by Si to form $Nd_{60}Fe_{30}Si_{10}$ alloy and when Fe in $Sm_{60}Fe_{30}Al_{10}$ is replaced by Co to form $Sm_{60}Co_{30}Al_{10}$ alloy (table 1). It is noted that the coercivity for the ribbon of $Nd_{60}Fe_{30}Al_{10}$ alloy melt-spun at 5 m s^{-1} decreased from ~3229kAm^{-1} at 40K to ~1262K at 5K. Decrease of coercivity was also observed for the ribbon of the same alloy melt-spun at 30 m s^{-1}. The decrease in coercivity was due to antiferromagnetic transition of the Nd phase (N èel temperature of Nd = 19K [16]).

$M(T, H)/f\ (T/\ T_c^{\text{cluster}})$ versus f $(T/\ T_c^{\text{cluster}})[H + \alpha M\ (T, H)]/T$ plots were constructed based on the magnetization curves of these amorphous $RE_{60}Fe_{30}Al_{10}$ ribbons taken at temperatures in the superparamagnetic regime (where anisotropy energy term $-D\sum_i[\overrightarrow{n_i}\cdot\overrightarrow{m_i}(T)]^2$ in Hamiltonian for cluster ferromagnetic model can be omitted). By molecular field approximation, the magnetization at temperature T and magnetic field H in the superparamagnetic regime can be expressed as the modified Langevin function with molecular field (αM) incorporated below [14]:

$$M(T, H) = N m_s f\left(\frac{T}{T_c^{\text{cluster}}}\right) \times L\left(\frac{m_s f(T/T_c^{\text{cluster}})[H + \alpha M(T, H)]}{k_B T}\right) \quad (3)$$

where N is the cluster density, α is the molecular field coefficient and k_B is the Boltzmann constant. $m_s f(T/T_c^{\text{cluster}})$ is the magnetic moment at temperature T (= $m(T)$). A universal curve should be obtained for each ribbon for appropriate values of T_c^{cluster} and α. The universal curve for the ribbon of $Dy_{60}Fe_{30}Al_{10}$ alloy melt-spun at 30 m s^{-1} is shown in figure 7. T_c^{cluster} and α thus obtained, and the T_c^{system} and m_s calculated according to the equations below are listed in table 1.

$$T_c^{\text{system}} = N m_s^2 f^2\left(\frac{T_c^{\text{system}}}{T_c^{\text{cluster}}}\right)\frac{\alpha}{3k_B} \quad (4)$$

$$m_s = \frac{3k_B}{M_0}\left(\frac{M(T, H)/f(T/T_c^{\text{cluster}})}{f(T/T_c^{\text{cluster}})([H + \alpha M(T, H)]/T)}\right) \quad (5)$$

Good agreement between the critical transition temperatures obtained by fitting and estimated experimentally shows that the magnetic behaviour of these amorphous $RE_{60}Fe_{30}Al_{10}$ ribbons can be well described by the cluster ferromagnetism model.

4. DISCUSSIONS

4.1. Effect of RE elements

T_c^{cluster} of ribbon of $Gd_{60}Fe_{30}Al_{10}$ alloy melt-spun at 5 m s^{-1} c was the highest among all the ribbons melt-spun at the same speed. Gd is an S-state RE ion, hence its anisotropy energy is not expected to be high as compared to other non-S-state RE element ions. The high T_c^{cluster} observed might be due to the presence of Gd with high Curie temperature (293.4 K). Variation of Curie temperature of RE_xFe_y compounds (e.g. RE_2Fe_{17} and $ReRe_2$) with RE ion involved also show a maximum value when RE = Gd [17] due to the effect of spin of RE ion (spin of Gd^{3+} ion = 7/2, largest among all the RE^{3+} ions).

T_c^{system} of the ribbons melt-spun at 5 and 30 m s^{-1} show similar dependence on RE elements present in the alloy, with maximum when RE = Nd and minimum when RE = Y. According to our Monte Carlo simulation results [1], low T_c^{system} is an indication of weak interactions between the c particles. Y is a non-magnetic atom and hence might not contribute any magnetic moment to the interaction.

High T_c^{system} of $Nd_{60}Fe_{30}Al_{10}$ ribbons is an indication of the very strong interactions that resulted in ferromagnetic coupling between the magnetic clusters. It is noticed from table 1 that the α value that signifies the strength of the interaction between the magnetic clusters of $Nd_{60}Fe_{30}Al_{10}$ ribbon is also the highest. Coupling constant $J_{RE–Fe}$ between the RE spin and Fe spin in $RE_2Fe_{14}B$ compounds is highest and hence the interaction is

strongest when RE = Nd [18]. If similar RE–Fe interaction exists in our amorphous $RE_{60}Fe_{30}Al_{10}$ ribbons and contributes to the interaction between the Fe-rich clusters, T_c^{system} that reflects the strength of interaction of the $Nd_{60}Fe_{30}Al_{10}$ ribbon is expected to be higher than other ribbons.

4.2. Effect of melt-spinning speed

T_c^{system} and T_c^{cluster} of the ribbons of all alloys melt-spun at 5 m s^{-1} were higher than those melt-spun at 30 m s^{-1}. T system corresponds to the strength of magnetic interaction between the magnetic clusters; higher the T_c^{system}, stronger the interaction. Cooling rate experienced by the ribbons melt-spun at 5 ms^{-1} is lower than the ribbons melt-spun at 30ms^{-1}. Formation of larger cluster or higher density of cluster at the lower cooling rate might decrease the average separation distance between the Fe-rich clusters which were scattered in the amorphous matrix, and hence promote the interactions between the magnetic clusters. Another possibility is that the RE crystallites of about 3 nm formed only at low melt-spinning speed of 5ms^{-1} might act as some kind of medium for the interaction between the Fe-rich clusters. Furthermore, concentration of Fe in the remaining amorphous phase might be enriched as RE phase precipitated out from the amorphous matrix and hence facilitating formation of the magnetic Fe-rich clusters. T_c^{system} is determined mainly by the composition of the clusters. Presence of a certain amount of RE atoms and Al atoms in the Fe-rich clusters are expected. Formation of RE crystallites at low melt-spinning speed (5 m s^{-1}) might decrease the amount of RE atoms in the clusters, leaving the clusters rich in an element of high Curie temperature—Fe (1040.2 K), thus elevating the Curie temperature of the whole cluster.

4.3. RKKY interactions

The Monte Carlo simulation results show that in order to have high coercivity, the anisotropy of the cluster system must be high [1]. There are two possibilities. The first possibility is that the clusters might be hard magnetic themselves. The second possibility is that there is some interaction between the RE small crystallites and the Fe-rich clusters that resulted in high anisotropy. From the magnetic behaviour and high T_c^{system} observed, strong interaction between the clusters is suggested. If the interaction existing in the system was dipole interaction, molecular field coefficient α should be equal to, and not greater than, 1. However, according to our Langevin fitting results, α for the $RE_{60}Fe_{30}Al_{10}$ ribbons are much greater than 1 (as listed in table 1) suggesting that RKKY-like interaction [19–21] might be present. Hence, the interactions between these amorphous Fe-rich magnetic clusters might involve certain degree of indirect exchange interaction mediated by the surrounding RE crystallites.

4.4. Coercivity mechanism

Table 1 shows high coercivity values (well above 1000 kA m^{-1}) were observed for ribbons based on Nd, Sm, Dy melt-spun at 30 m s^{-1}. Coercivity values of Y- and Gd-based ribbons remain low (at below 100 kA m^{-1}) at temperatures down to 5 K. Simulated

hysteresis loops using the Monte Carlo method based on cluster ferromagnetism model shows that coercivity is determined mainly by the magnetic anisotropy energy of the cluster phase at low temperatures [1]. Generally, the main contribution to magnetic anisotropy in permanent magnet materials like RE–Fe–B and RE–Co is due to the single-ion crystal field-induced anisotropy of the magnetic RE atoms which arises as a consequence of the interaction between the electrostatic field of the charges surrounding the 4f electrons and the asymmetric charge-cloud of these 4f electrons [22]. The difference in shape of the 4f charge-cloud is reflected by the sign of the second-order Stevens factor (α_J) [23,24]. This crystal field-induced anisotropy is absent in materials based on Gd that has a zero α_J [22]. It was noticed that coercivity of the largely amorphous $RE_{60}Fe_{30}Al_{10}$ ribbon based on Gd with zero α_J remains low. In contrast, the α_J of the RE material on which the ribbons with high coercivity are based (e.g. Nd, Sm and Dy) are none zero (either positive or negative). Results of amorphous $(Gd_{0.75}RE_{0.25})_{19}Co_{81}$ films based on the single-ion anisotropy model [25] also show an increase of uniaxial anisotropy constant K_u and hence anisotropy energy with increasing α_J of RE (either positively or negatively). A relationship between the value of α_J (either zero or non-zero) and the magnitude of coercivity at low temperature is suggested.

In addition, considering the large magnetostriction observed for RE–Fe compounds [26], magnetostriction may contribute to the magnetic anisotropy and hence high coercivity values observed for these ribbons of $RE_{60}Fe_{30}Al_{10}$.

5. CONCLUSIONS

Ribbon of $Dy_{60}Fe_{30}Al_{10}$ alloy melt-spun at 5 m s^{-1} contained Dy crystallites of diameter around 3 nm, and Fe-rich clusters with diameter of about 2.5 nm. Amorphous ribbons of $RE_{60}Fe_{30}Al_{10}$ alloys were paramagnetic at temperatures above T_c^{cluster}, superparamagnetic at temperatures between T_c^{system} and T_c^{cluster}, ferromagnetic with low coercivity at temperatures between T_{block} and T_c^{system}, ferromagnetic with high coercivity at temperatures below T_{block} (except RE = Gd and Y), a sequence expected from the cluster ferromagnetism model. T_c^{system}, T_c^{system} and T_{block} for ribbons of $RE_{60}Fe_{30}Al_{10}$ alloys estimated from temperature dependence of inverse susceptibility, reduced magnetization and coercivity agreed well with those obtained from fitting by modified Langevin function based on the cluster ferromagnetism model. $Nd_{60}Fe_{30}Al_{10}$ ribbons exhibit the highest T_c^{system} among all the ribbons. T_c^{system} and T cluster c of the ribbons melt-spun at 5m s^{-1} were higher than those of the ribbon melt-spun at 30 ms^{-1}. Ribbons of $RE_{60}Fe_{30}Al_{10}$ alloys with RE of non-zero second-order Stevens factor (α_J) exhibit high coercivity at temperatures below T_{block}.

REFERENCES

[1] Wang L, Ding J, Kong H Z, Li Y and Feng Y P 2001 *Phys. Rev*. B **64** 214410
[2] Hansen P 1991 *Handbook of Magnetic Materials* vol 6, ed K H J Buschow (Amsterdam: Elsevier) chapter 4
[3] Graczyk J F 1978 J. Appl. Phys. **48** 1738
[4] Tsunashima S H, Takagi S H, Kamegaki K, Fujii T and Uchiyama S 1978 *IEEE Trans. Magn.* **14** 844
[5] Chaudhari P and Cronemeyer D C 1975 AIP *Conf. Proc*. **29** 113
[6] Meiklejohn W H, Luborsky F Eand Frischmann P G 1987 *IEEE Trans. Magn*. **23** (5) 2272
[7] Inoue A, Takeuchi A and Zhang T 1998 *Metall. Mater. Trans*. A **29** 1779
[8] Yoshiike S, Adachi H, Ichinose H, Tokumitsu K, Ino H and Siratori K 1998 *Mater. T. JIM* **39** (1) 102
[9] Ding J, Li Y and Wang X Z 1999 J. Phys. D: *Appl. Phys.* **32** 713
[10] Wang L, Ding J, Li Y, Kong H Z, Feng Y P and Wang X Z 2000 *J. Phys.: Condens. Matter* **12** 4253
[11] Kong H Z, Li Y and Ding J 2001 *Scripta Mater*. **44** 829
[12] Kong H Z, Ding J, Wang Land Li Y *2001 IEEE Trans. Magn.* **37** (4) 2500
[13] Ortega-Hertogs R J, Inoue A and Rao K V 2001 *Scripta Mater*. **44** 1333
[14] Wang L, Ding J, Li Y, Feng Y P, Phuc N X and Dan N H 2001 *J. Appl. Phys*. **89** (12) 8046
[15] Kumar D, Narayan J, Kvit A V, Sharma A K and Sankar J 2001 J. *Magn. Magn. Mater.* **232** 161
[16] Legvold S 1980 Ferromagnetic Materials vol 1, ed E P Wohlfarth (Amsterdam: North-Holland) p 189
[17] Franse J J M and Radwanski R J 1993 *Handbook of Magnetic Materials* vol 7, ed K H J Buschow (Amsterdam: Elsevier) p 395
[18] Belorizky E, Fremy M A, Gavigan J P, Givord D and Li H S 1987 J. *Appl. Phys.* **61** 3971
[19] Rudermann M A and Kittel C 1954 *Phys. Rev*. **96** 99
[20] Kasuya T *1956 Prog. Theor. Phys*. **16** 45
[21] Yosida K 1957 *Phys. Rev*. **106** 893
[22] Buschow K H J 1988 Ferromagnetic Materials vol 4, ed E P Wohlfarth and K H J Buschow (Amsterdam: Elsevier) pp 48–9
[23] Ballou R 1992 *Proc. Magnetism, Magnetic Materials and Their Applications* ed F Leccabue and J L Sanchez Llamazares (Bristol: Institute of Physics Publishing) pp 30–1
[24] Hutchings M T 1964 *Solid State Physics* vol 16, ed F Seitz and D Turnbull (New York: Academic) p 227
[25] Suzuki Y, Takayama S, Kirino F and Ohta N 1987 *IEEE Trans. Magn*. **23** (5) 2275
[26] Clark A E 1980 Ferromagnetic Materials vol 1, ed E P Wohlfarth (Amsterdam: North-Holland) pp 533–4

List of Figures

List of Tables

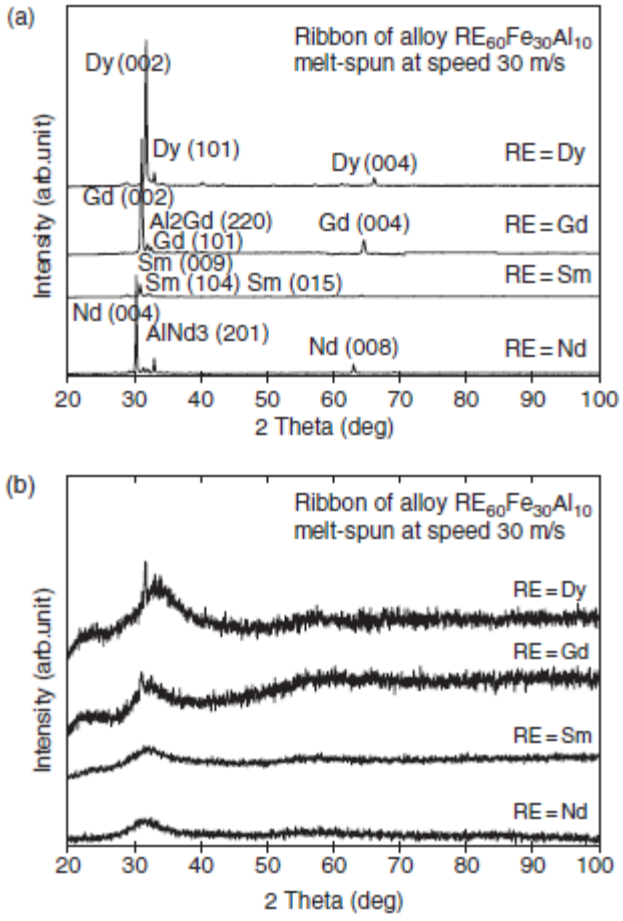
(a)
Ribbon of alloy $RE_{60}Fe_{30}Al_{10}$
melt-spun at speed 30 m/s
Dy (002)
Dy (101)
Dy (004)
RE = Dy
Gd (002)
Al2Gd (220)
Gd (101)
Gd (004)
RE = Gd
Sm (009)
Sm (104) Sm (015)
RE = Sm
Nd (004)
AlNd3 (201)
Nd (008)
RE = Nd
Intensity (arb.unit)
20 30 40 50 60 70 80 90 100
2 Theta (deg)
(b)
Ribbon of alloy $RE_{60}Fe_{30}Al_{10}$
melt-spun at speed 30 m/s
RE = Dy
RE = Gd
RE = Sm
RE = Nd
Intensity (arb.unit)
20 30 40 50 60 70 80 90 100
2 Theta (deg)

Figure 1

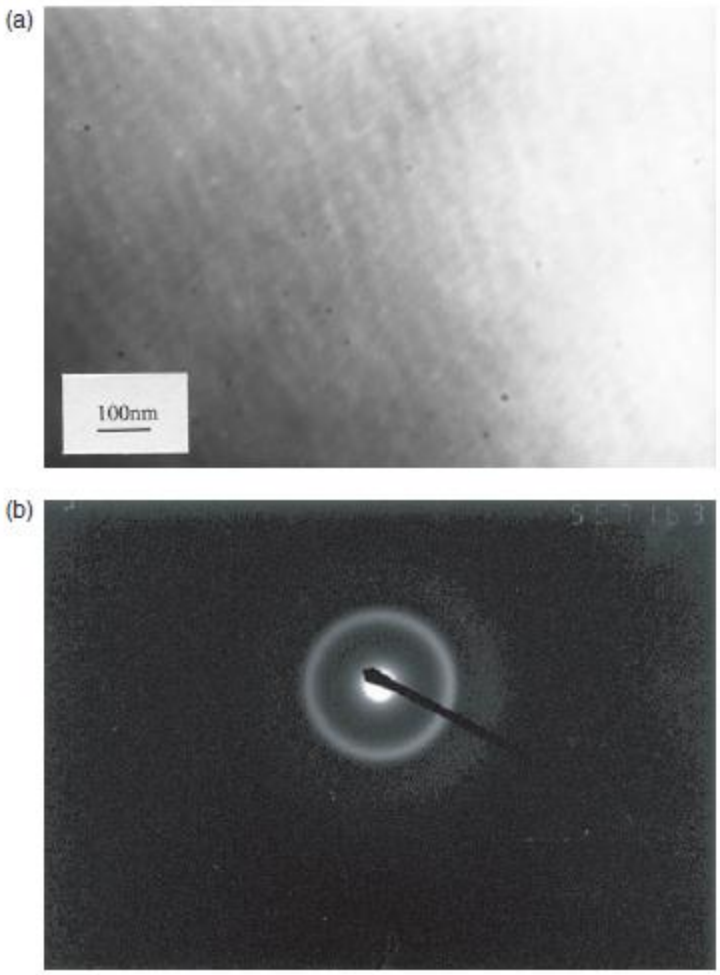

Figure 2

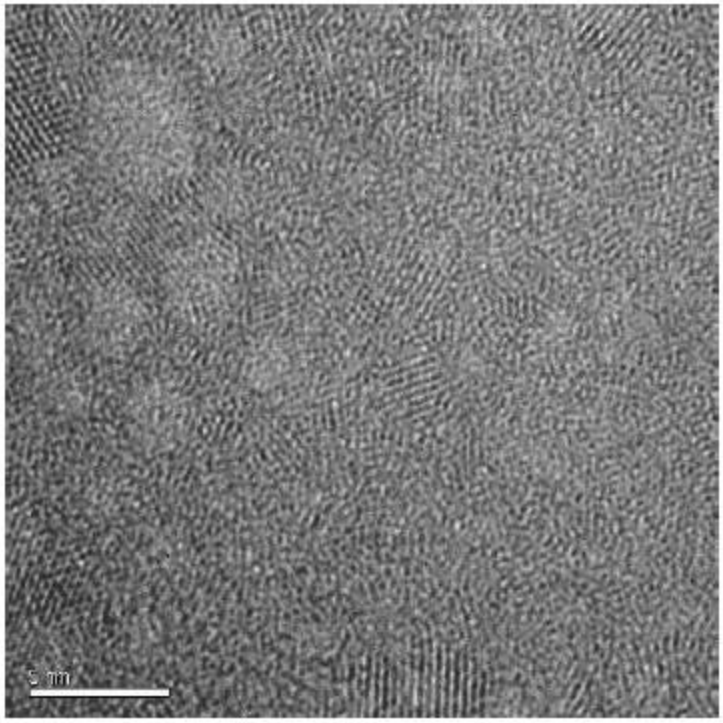

Figure 3

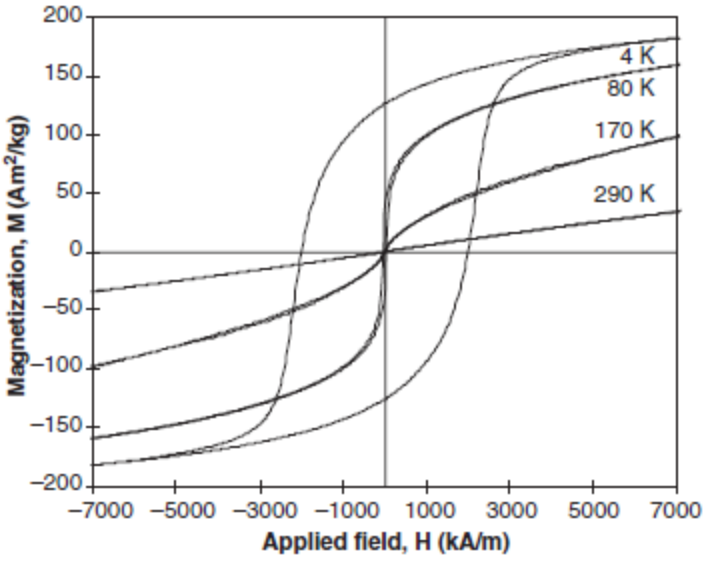
200
150
100
50
0
−50
−100
−150
−200
Magnetization, M (Am²/kg)
4 K
80 K
170 K
290 K
−7000
−5000
−3000
−1000
1000
3000
5000
7000
Applied field, H (kA/m)

Figure 4

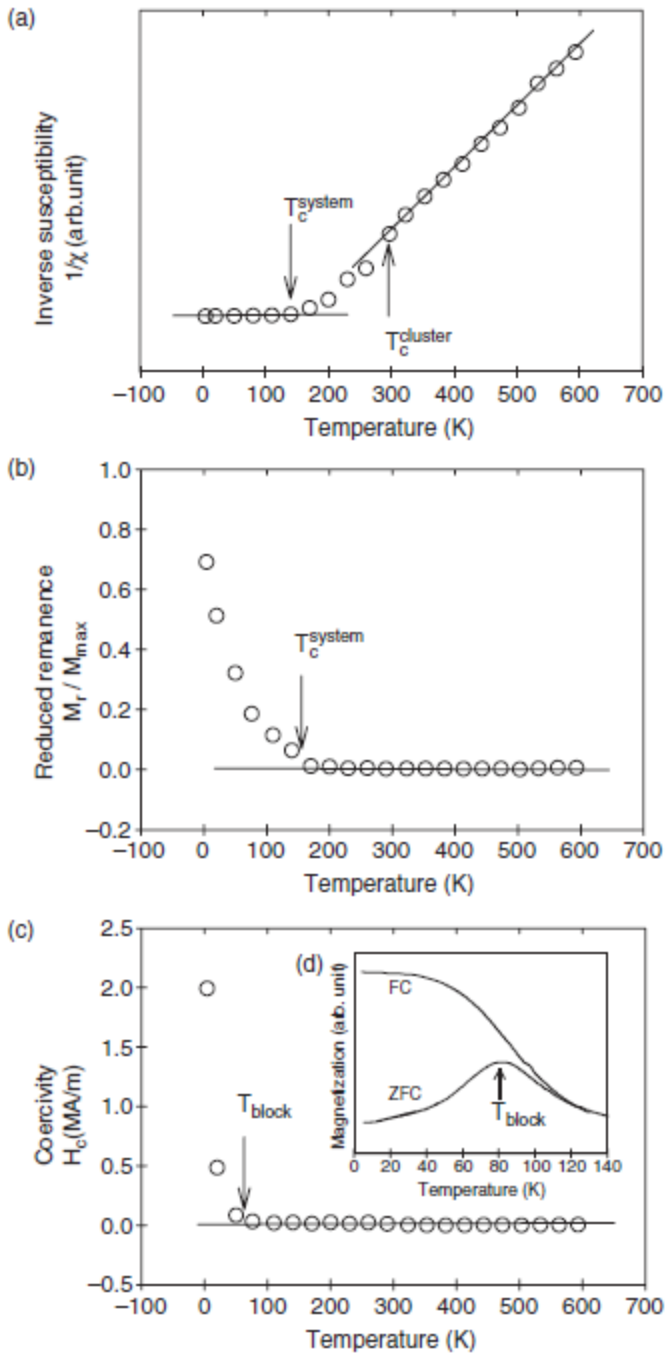
(a)
Inverse susceptibility
1/χ (arb.unit)
T_c^{system}
$T_c^{cluster}$
−100 0 100 200 300 400 500 600 700
Temperature (K)
(b)
Reduced remanence
M_r / M_{max}
1.0 0.8 0.6 0.4 0.2 0.0 −0.2
T_c^{system}
−100 0 100 200 300 400 500 600 700
Temperature (K)
(c)
Coercivity
H_c(MA/m)
2.5 2.0 1.5 1.0 0.5 0.0 −0.5
T_{block}
(d)
Magnetization (arb. unit)
FC
ZFC
T_{block}
0 20 40 60 80 100 120 140
Temperature (K)
−100 0 100 200 300 400 500 600 700
Temperature (K)

Figure 5

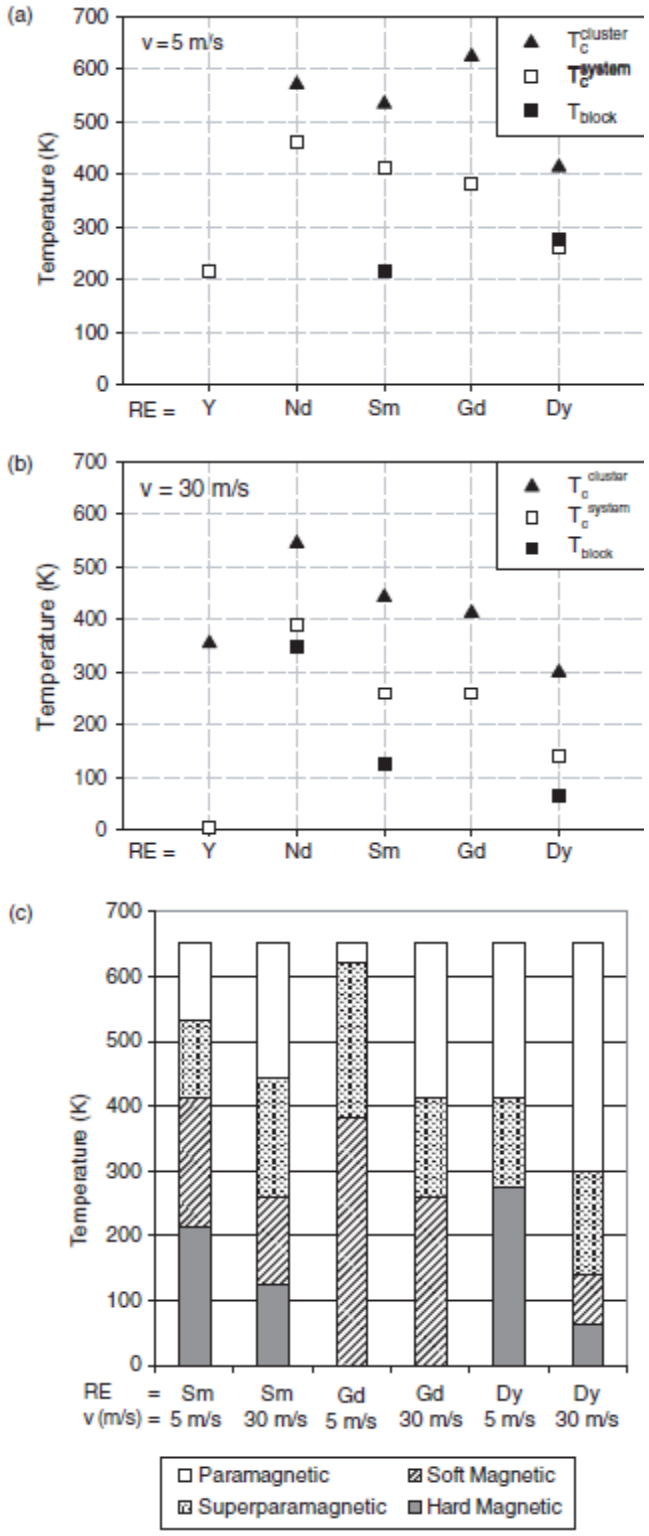
(a)
v = 5 m/s
$T_c^{cluster}$
T_c^{system}
T_{block}
Temperature (K)
700
600
500
400
300
200
100
0
RE = Y Nd Sm Gd Dy
(b)
v = 30 m/s
$T_c^{cluster}$
T_c^{system}
T_{block}
Temperature (K)
700
600
500
400
300
200
100
0
RE = Y Nd Sm Gd Dy
(c)
Temperature (K)
700
600
500
400
300
200
100
0
RE = Sm Sm Gd Gd Dy Dy
v (m/s) = 5 m/s 30 m/s 5 m/s 30 m/s 5 m/s 30 m/s
Paramagnetic
Soft Magnetic
Superparamagnetic
Hard Magnetic

Figure 6

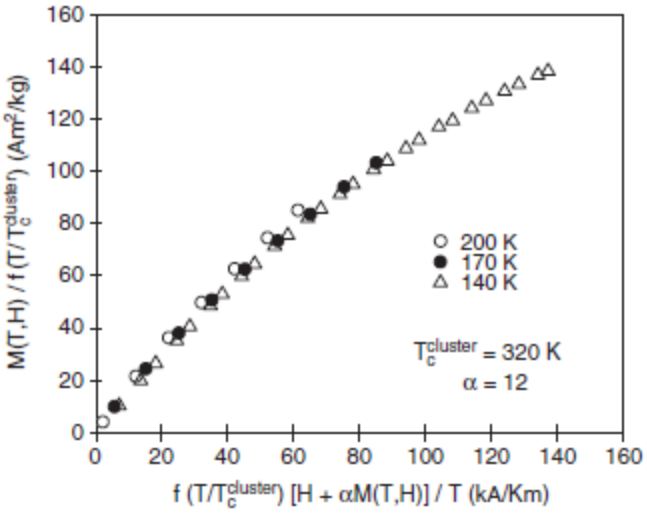
160
140
120
100
80
60
40
20
0
0
20
40
60
80
100
120
140
160
M(T,H) / f (T/T$_c^{cluster}$) (Am^2/kg)
f (T/T$_c^{cluster}$) [H + αM(T,H)] / T (kA/Km)
200 K
170 K
140 K
T$_c^{cluster}$ = 320 K
α = 12

Figure 7

Table 1. T_{block}, T_c^{system} and $T_c^{cluster}$ of the ribbons of $RE_{60}Fe_{30}Al_{10}$ alloys estimated experimentally and by fitting.

			Experimentally determined			Determined by fitting			
Alloy	v ($m\,s^{-1}$)	H_c at 5 K (or as-stated) ($kA\,m^{-1}$)	T_c^{system} (K)	$T_c^{cluster}$ (K)	T_{block} (K)	α —	m_s (μ_B)	T_c^{system} (K)	$T_c^{cluster}$ (K)
$Dy_{60}Fe_{30}Al_{10}$	5	232 (at 80 K)	260	413	275	—	—	—	—
	30	1992.4	140	300	65	12	47	135	320
$Gd_{60}Fe_{30}Al_{10}$	5	3.62 (at 290 K)	383	623	—	—	—	—	—
	30	7.67	260	413	—	21	660	306	500
$Sm_{60}Fe_{30}Al_{10}$	5	2677.95	413	533	215	—	—	—	—
	30	3305.2	260	443	125	18	880	—	630
$Y_{60}Fe_{30}Al_{10}$ [1]	5	~95	215	—	—	61	600	135	500
	30	~95	6	355	13	3	150	8	360
$Nd_{60}Fe_{30}Al_{10}$ [1]	5	~3239 (at 40 K) ~1262 (at 5 K)	460	570	—	—	—	—	—
	30	~2467 (at 80 K) ~597 (at 20 K)	390	545	—	475	15	397	520
$Nd_{60}Fe_{30}Si_{10}$	30	2648.2 (at 80 K)	443	533	338	—	—	—	—
$Sm_{60}Co_{30}Al_{10}$	30	1012.8 (at 20 K) >7162 (at 5 K)	40	50	45	—	—	—	—

Table 1